Journal of Fluorescence (2018) 28:1363–1370
https://doi.org/10.1007/s10895-018-2299-z

ORIGINAL ARTICLE

A Highly Selective Fluorescent Chemosensor for Detecting Indium(III) with a Low Detection Limit and its Application

Cheal Kim[1] · Ju Byeong Chae[1]

Received: 5 July 2018 / Accepted: 12 September 2018 / Published online: 24 September 2018

Abstract

A highly selective chemosensor **BHC** ((E)-N-benzhydryl-2-((2-hydroxynaphthalen-1-yl)methylene)hydrazine-1-carbothioamide) for detecting indium(III) was synthesized. Sensor **BHC** can detect In(III) by a fluorescence turn-on method. The detection limit was analyzed to be 0.89 μM. Importantly, this value is the lowest among those previously known for fluorescent turn-on In(III) chemosensors. Based on the analytical methods like ESI-mass, Job plot, and theoretical calculations, the detection mechanism for In(III) was illustrated to be chelation-enhanced fluorescence (CHEF) effect. Additionally, sensor **BHC** was successfully applied to test strips.

Keywords Fluorescence · Chemosensor · Indium · Test strip · Theoretical calculations

Introduction

Indium is one of the elements of group 13 and its consumption has been gradually increased [1]. Most usage of indium is in semiconductor-related applications [2]. Apart from these applications, the pollution from it can affect severe health problems [3]. Although it has no biological role in human body, its effects have been reported to be toxic to humans, causing kidney disease and interference towards iron metabolism [4]. Therefore, it is needed to develop efficient detecting strategies for indium [5–7].

There are several analytical tools for the detection of a broad range of metal ions like AAS, ICP-AES (inductively coupled plasma atomic emission spectrometry), and other electrochemical methods (Absence of Gradients and Nernstian Equilibrium Stripping) [8–11]. However, they need complex procedures and sample pre-treatment and the costs are relatively high [12]. In contrast, chemosensors have been noted for its easy usage, fast response and cost-effective advantages [13–17].

Owing to similar properties of the 13 group elements, Al^{3+} and Ga^{3+}, it is a challenge to distinguish In^{3+} from them. Until now, many chemosensors for Al^{3+} and Ga^{3+} were developed, but a few for In^{3+} [18–22]. Moreover, some of the In^{3+} chemosensors have difficulty in detecting In^{3+} because they are inhibited by Al^{3+} and Ga^{3+} or detected via quenching response which is a less preferred method [2, 4, 5, 7]. Thus, the chemosensor capable of sensing In^{3+} without interferences especially from Al^{3+} and Ga^{3+} with a turn-on response is highly demanded.

The benzhydryl isothiocyanate with hydrazine moiety could offer binding site to metal ions as well as act as a linker. A naphthol moiety is widely used as a fluorophore because of its unique photophysical property [23]. Therefore, we expected that the linkage of the two functional moieties can induce a unique optical change towards a specific metal ion.

Herein, we present a highly selective and sensitive fluorescence probe **BHC**, which can detect In^{3+} via a fluorescence turn-on. Importantly, it can distinguish In^{3+} from the same group metals, Al^{3+} and Ga^{3+}, without interferences. In addition, the binding mode and sensing mechanism for In^{3+} were explained, based on the spectroscopic studies and theoretical calculations.

Electronic supplementary material The online version of this article (https://doi.org/10.1007/s10895-018-2299-z) contains supplementary material, which is available to authorized users.

✉ Cheal Kim
chealkim@seoultech.ac.kr

[1] Department of Fine Chem, Seoul National University of Science and Technology (SNUT), Seoul 138-743, South Korea

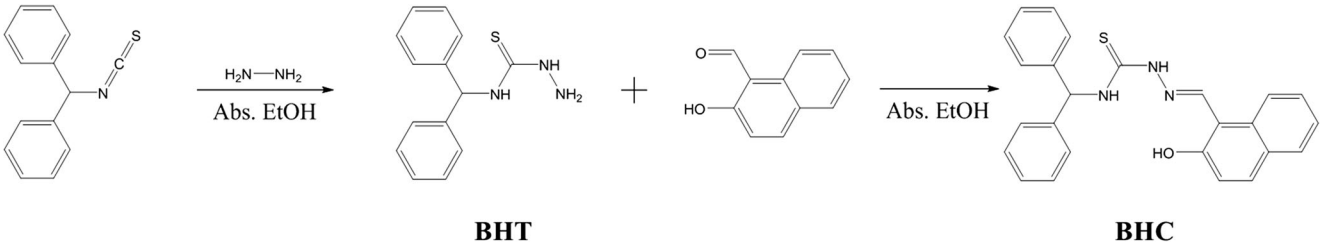

Scheme 1 Synthesis of compound **BHC**

Experimental Section

General Information

Chemicals were provided commercially. Stock solutions of the cations (Cd^{2+}, Al^{3+}, K^{+}, Ga^{3+}, Ca^{2+}, In^{3+}, Zn^{2+}, Na^{+}, Cu^{2+}, Ni^{2+}, Fe^{3+}, Co^{2+}, Hg^{2+}, Mg^{2+}, Cr^{3+}, Pb^{2+}, Mn^{2+} and Ag^{+}) were prepared using nitrate salts in dimethylsulfoxide (20 mM). Perchlorate salt was used for the Fe^{2+} stock solution. NMR data were measured using a Varian spectrometer (400 MHz). A Perkin Elmer spectrometer (Lambda 2S UV/Vis) was used for absorption spectra. ESI-mass data were gained on a Thermo Finnigan LCQTM instrument. A Perkin-Elmer spectrometer (LS45) was used for fluorescence data, and the slit width for excitation and emission was 10 nm.

Synthesis and Characterization of BHT (1-benzhydrylthiourea)

Benzhydryl isothiocyanate (1.12 g, 5.0 mmol) and hydrazine monohydrate (334 μL, 5.5 mmol) were dissolved in 10 mL of absolute ethanol and stirred for 6 h until white precipitate formed. It was filtered and washed with chilly ethanol and diethylether. Yield: 0.87 g (60%). ^{1}H NMR (DMSO-d_6, 400 MHz, ppm): δ 8.96 (s, 1H), 8.37 (s, 1H), 7.28 (m, 10H), 6.76 (s, 1H), 4.64 (s, 2H).

Synthesis and Characterization of BHC ((E) -N-benzhydryl-2-((2-hydroxynaphthalen-1-yl) methylene)hydrazine-1-carbothioamide)

BHT (480 mg, 2.0 mmol) and 2-hydroxy-1-naphthaldehyde (360 mg, 2.1 mmol) were dissolved in 5 mL of absolute ethanol and stirred for 1 day until pale yellow powder formed. It was filtered and washed with chilly ethanol and diethylether. Yield: 0.46 g (56%). ^{1}H NMR ($CDCl_3$, 400 MHz, ppm): δ 10.62 (s, 1H), 10.23 (s, 1H), 9.00 (s, 1H), 7.92 (d, J = 8.4, 1H), 7.83 (d, J = 9.2 Hz, 1H), 7.79 (d, J = 8.4 Hz, 1H), 7.54 (t, J = 7.8 Hz, 1H), 7.4 (t, J = 7.6 Hz, 1H), 7.32 (m, 11H), 7.17 (d, J = 8.8 Hz, 1H), 6.92 (d, J = 8.4 Hz, 1H), ^{13}C NMR (DMSO-d_6, 100 MHz, ppm): δ = 176.73 (1C), 156.70 (1C), 142.51 (1C), 141.90 (2C), 132.50 (1C), 131.40 (1C), 128.82 (1C), 128.55 (4C), 128.14 (1C), 127.61 (1C), 127.37 (4C), 127.23 (2C), 123.47 (1C), 122.84 (1C), 118.42 (1C), 110,11 (1C), 60.70 (1C). Positive-ion ESI-MS: m/z calcd, for [2·**BHC** + Na^{+}]$^{+}$, $C_{50}H_{42}N_6O_2S_2$ + Na^{+}, 845.27; found, 845.18.

Fluorescence and UV-vis Titrations of BHC with In^{3+}

A stock solution of **BHC** was prepared in dimethylsulfoxide (DMSO, 1×10^{-2} M). 3 μL of it was diluted to 3 mL of DMSO for 10 μM concentration. A stock solution (2×10^{-2} M) of $In(NO_3)_3$ was prepared in DMSO. For the fluorescence titration, 1.5–37.5 μL of the In^{3+} solution was taken and mixed with **BHC**. 1.5–19.5 μL of the In^{3+} solution was added to the solution of **BHC** for UV-vis titration. Both fluorescence and UV-vis spectra were measured.

Quantum Yield of BHC and BHC-In^{3+}

Quantum yield (Φ) was calculated by using fluorescein (Φ_F = 0.92 in basic ethanol) as a standard fluorophore [24]. The equation of quantum yield is as follows [25]:

$$\Phi_{F(X)} = \Phi_{F(S)} \left(A_S F_X / A_X F_S\right) \left(n_X / n_S\right)^2$$

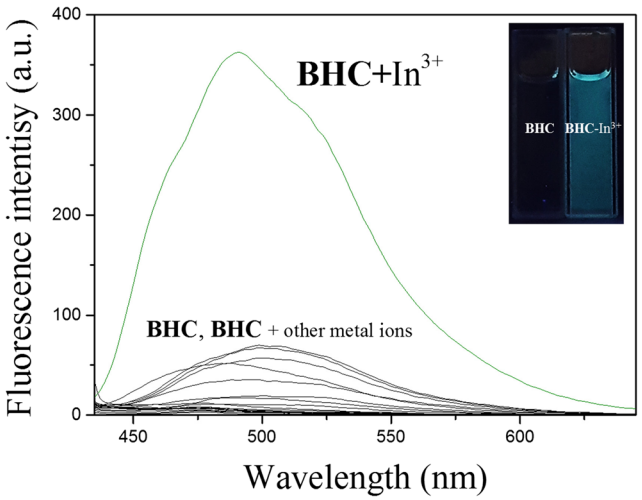

Fig. 1 Fluorescence spectra of **BHC** (10 μM) with various metal ions (23 equiv). Excitation wavelength: 416 nm

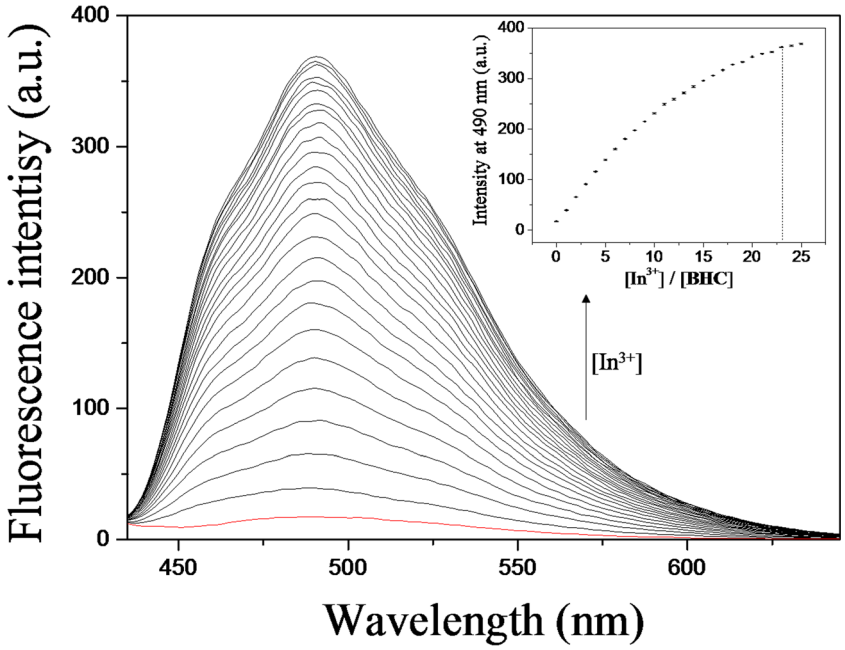

Fig. 2 Changes in fluorescence emission spectra when In^{3+} was added into sensor **BHC** (10 μM). Inset: fluorescence intensity at 490 nm (0–25 equiv). Excitation wavelength: 416 nm. Error bars represent standard deviations from three repeated experiments

Where the meaning of each abbreviation is

Φ_F	fluorescence quantum yield
A	Absorbance
F	The area of fluorescence emission curve
n	Refractive index of the solvent
s	standard
x	unknown

Job Plot Measurement of BHC with In^{3+}

160 μL of a **BHC** stock solution (DMSO, 1×10^{-2} M) was diluted to 39.84 mL DMSO for 40 μM concentration. 80 μL of an In^{3+} stock solution (DMSO, 2×10^{-2} M) was diluted to 39.92 mL DMSO for 40 μM concentration. Both solutions were mixed from the molar fractions of 0.1 to 0.9 while maintaining a constant overall concentration (40 μM). The emission spectrum of each solution was measured.

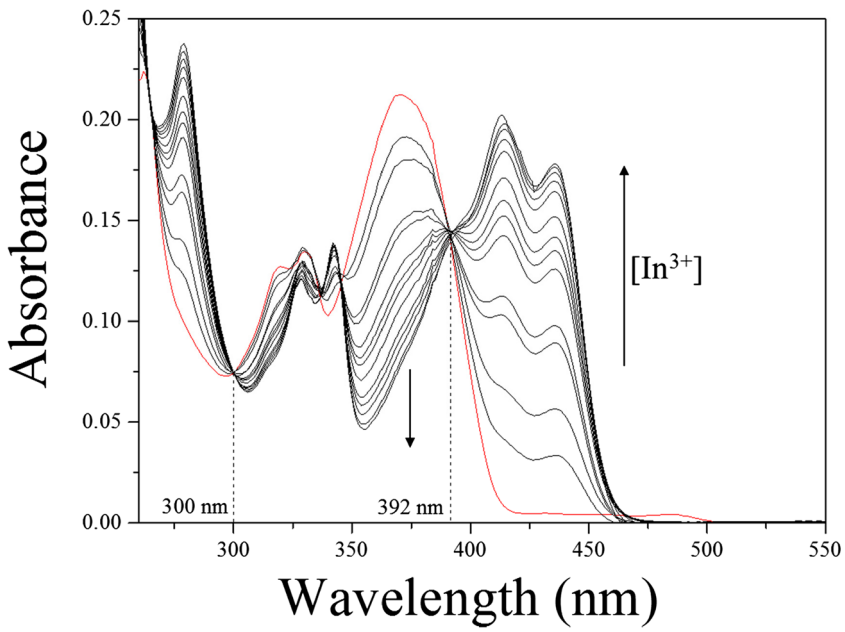

Fig. 3 Changes in UV-vis spectra when In^{3+} was added into sensor **BHC** solution (10 μM)

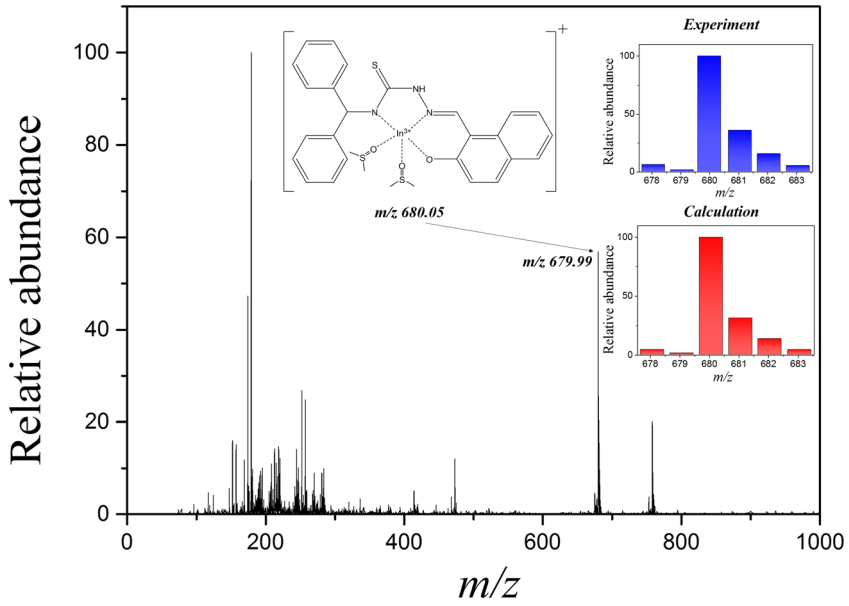

Fig. 4 Positive-ion ESI-MS spectrum of **BHC**-In^{3+} (100 μM, 1 equiv. of In^{3+})

Competition Experiment

34.5 μL of various metal-ion stock solutions dissolved in DMSO (Cd^{2+}, Al^{3+}, K^{+}, Ga^{3+}, Ca^{2+}, In^{3+}, Zn^{2+}, Na^{+}, Cu^{2+}, Ni^{2+}, Fe^{3+}, Co^{2+}, Hg^{2+}, Mg^{2+}, Cr^{3+}, Pb^{2+}, Mn^{2+} and Ag^{+}, 20 mM) were diluted to 3 mL of DMSO (23 equiv). The same amount of an In^{3+} stock solution was added to each solution. A stock solution of **BHC** (10 mM, 3 μL) was added to them and mixed. The emission spectrum of each solution was measured.

Fluorescence Test Kit

Filter papers were immersed to 700 mM of **BHC** solution (1 mL, DMSO). After they were dried in the oven, various amounts (10, 20, 50, 100, and 200 μM) of an In^{3+} stock solution were applied to them for determining the lowest visible detection limit. The test kit prepared above was also applied to 20 μM of various metal solutions (Cd^{2+}, Al^{3+}, K^{+}, Ga^{3+}, Ca^{2+}, In^{3+}, Zn^{2+}, Na^{+}, Cu^{2+}, Ni^{2+}, Fe^{3+}, Co^{2+}, Hg^{2+}, Mg^{2+}, Cr^{3+}, Pb^{2+}, Mn^{2+} and Ag^{+}).

Theoretical Studies

Energy-optimized structures of **BHC** and **BHC**-In^{3+} complex were calculated by density functional theory (DFT) using Gaussian 09 W program [26]. The hybrid functional was Becke, 3-parameter, Lee-Yang-Parr (B3LYP) and the basis set was 6-31G(d,p) [27–30]. All atoms except In^{3+} were applied to 6-31G(d,p) while LANL2DZ basis set was used as effective core potential (ECP) for In^{3+} [31–33]. Since imaginary frequency was not found in optimized structures of **BHC** and **BHC**-In^{3+}, their geometries represented local minima. CPCM was used for considering solvent effect of DMSO

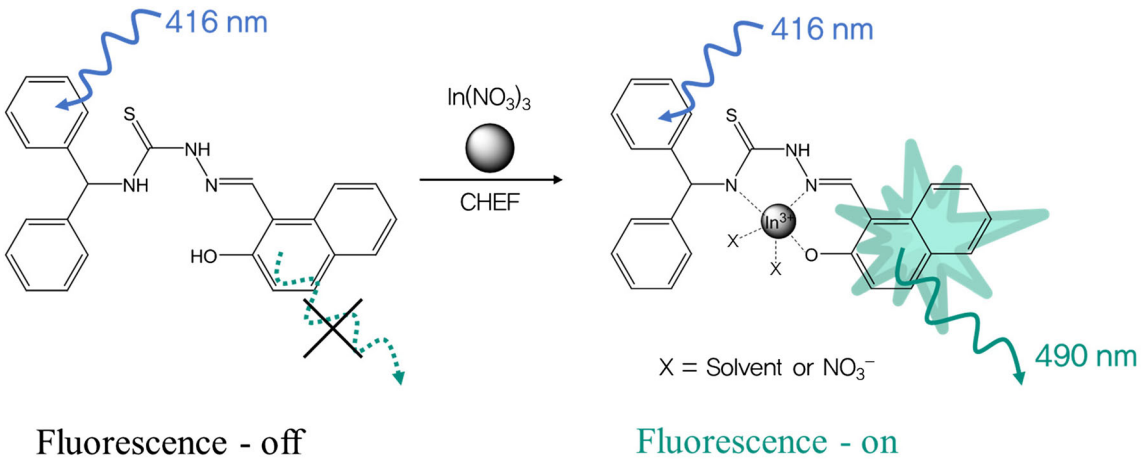

Scheme 2 Fluorescence turn-on mechanism and proposed binding structure of **BHC**-In^{3+}

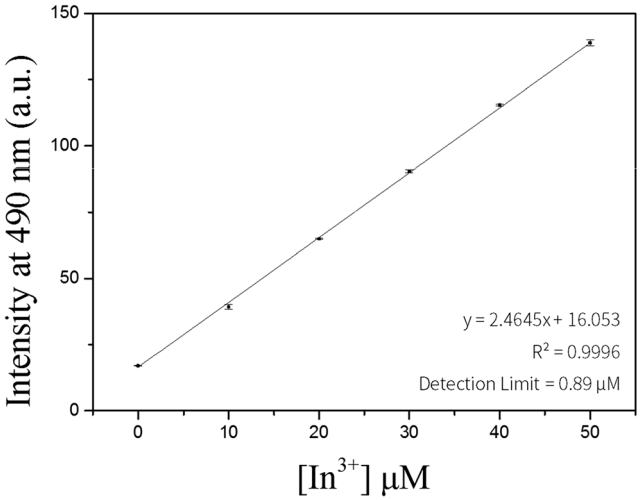

Fig. 5 Detection limit of **BHC** toward In^{3+} based on 3σ/slope. Error bars represent standard deviations from three repeated experiments

[34, 35]. According to energy-optimized structures of sensor **BHC** and **BHC**-In^{3+} complex, the UV-vis transition studies were confirmed using TD-DFT (time-dependent DFT) method with thirty lowest singlet states.

Results and Discussion

By the nucleophilic addition reaction of benzhydryl isothiocyanate and hydrazine, compound **BHT** was synthesized. Compound **BHC** was obtained from the condensation reaction of **BHT** and 2-hydroxy-1-naphthalaldehyde (Scheme 1). It was fully characterized through ^{1}H and ^{13}C NMR and ESI-MS analyses (Figs. S1-S3).

In order to study the sensing ability of compound **BHC** towards various metals, fluorescence spectra were measured with the excitation wavelength of 416 nm (Fig. 1). Most metals did not show critical fluorescence change. In contrast, only In^{3+} displayed a remarkable increase of the fluorescence emission at 490 nm. This obvious change indicated that sensor **BHC** could detect In^{3+} by fluorescence turn-on. For investigating the counter-anion effect, we also used $In_2(SO_4)_3$ instead of indium nitrate. Indium sulfate also showed nearly identical fluorescence enhancement as done with indium nitrate.

To investigate binding properties, fluorescence titration was achieved (Fig. 2). As the amount of In^{3+} increased, fluorescence emission at 490 nm was constantly increased. Quantum yields (Φ) of **BHC** and **BHC**-In^{3+} were calculated to be 0.0563 and 0.147. The binding interaction between **BHC** and In^{3+} was further studied with UV-vis titration (Fig. 3). The increase of In^{3+} induced absorption spectral changes with two defined isosbestic points at 300 nm and 392 nm, and it implies that only one species is present at the isosbestic point.

For the determination of binding stoichiometry of sensor **BHC** and In^{3+}, Job plot experiment was achieved (Fig. S4). The highest fluorescence intensity appeared at the point where the mole fraction was 0.5. It indicated that sensor **BHC** and

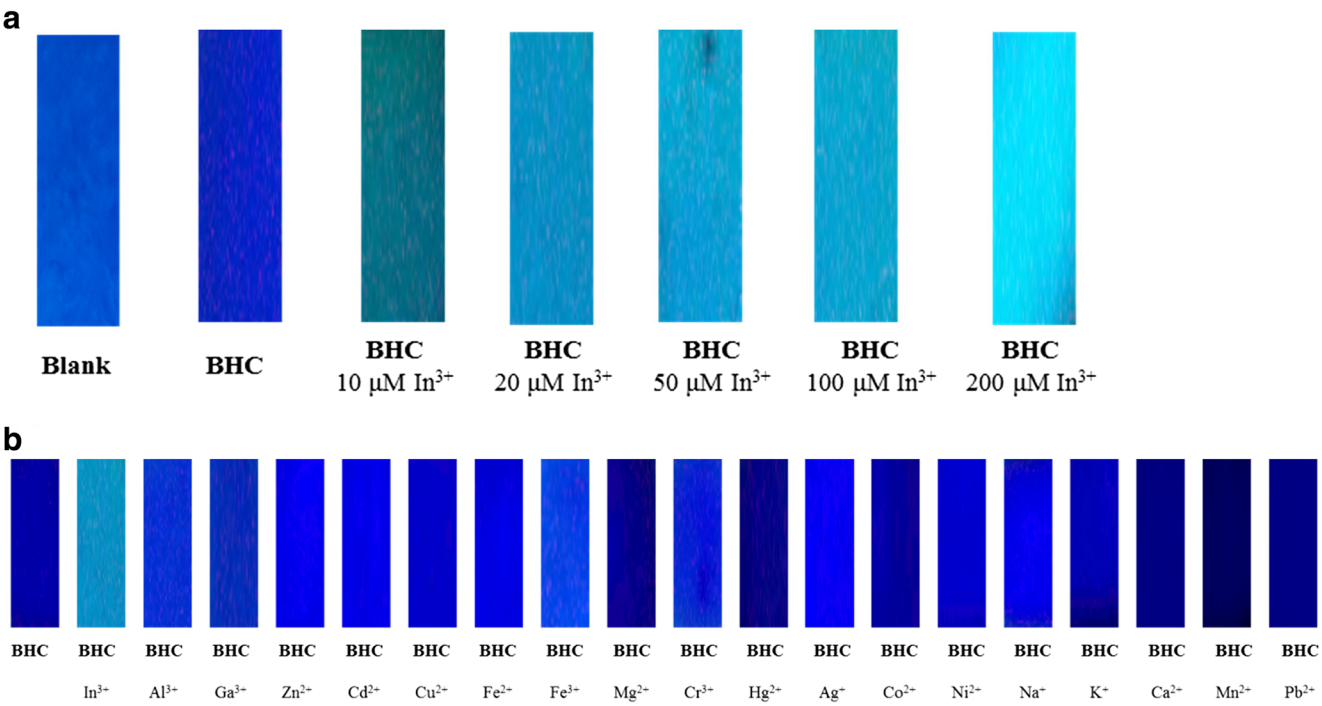

Fig. 6 Photographs of the test strips coated with sensor **BHC**. **a** Sensor **BHC**-test strips immersed in various concentrations of In^{3+} (0–200 μM). **b** Sensor **BHC**-test strips immersed in 20 μM of various metal ion solutions

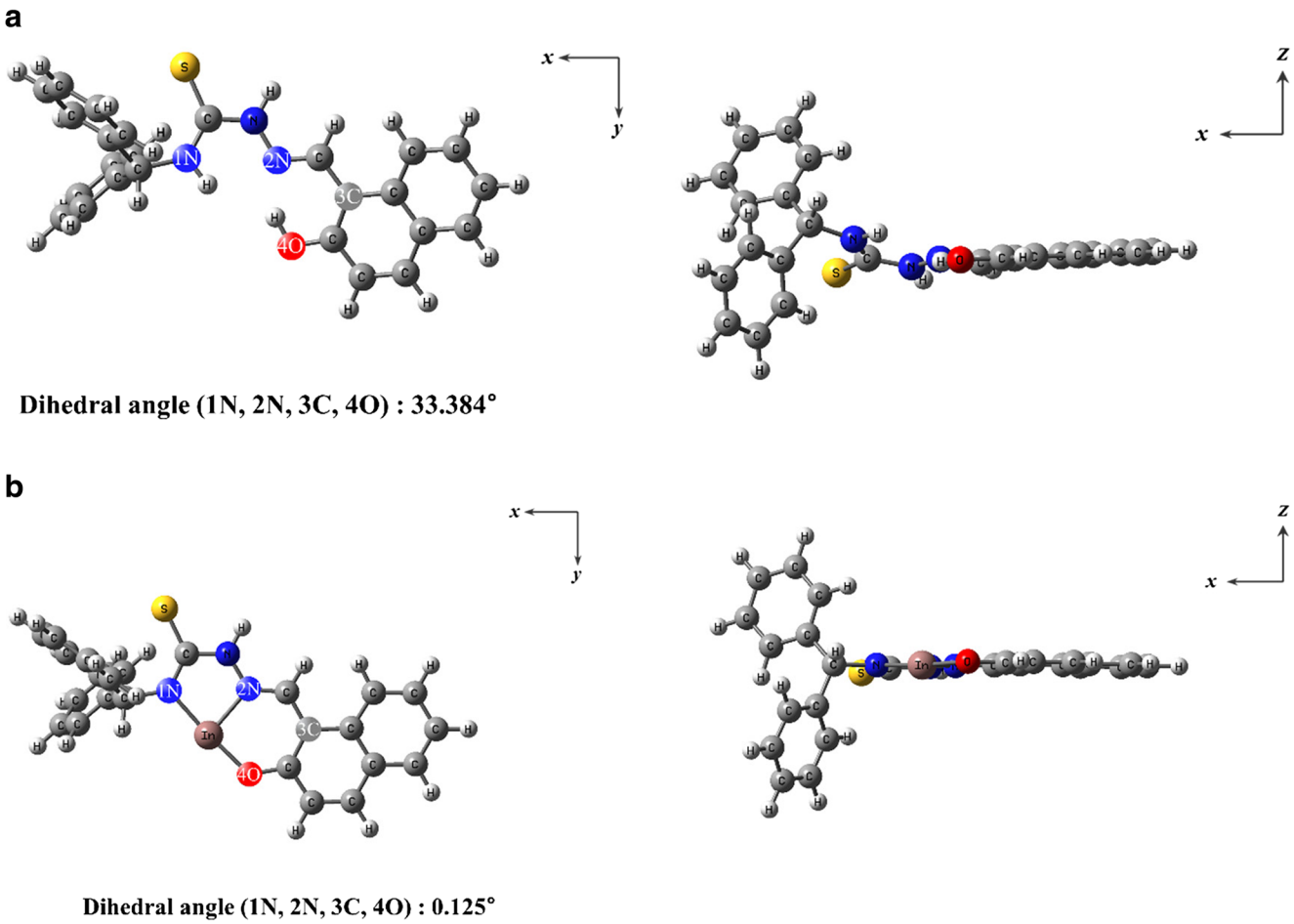

Fig. 7 Energy-optimized structure of (**a**) sensor **BHC** and (**b**) **BHC**-In^{3+} complex

In^{3+} were combined in a 1 to 1 ratio. To support the binding interaction between **BHC** and In^{3+}, positive-ion ESI-MS experiment was executed (Fig. 4). The peak of $m/z = 679.99$ was suggestive of **BHC**-$2H^{+}$+In^{3+} (calcd, $m/z = 680.05$). Its isotope pattern was well matched with the calculated value, supporting the 1: 1 binding stoichiometry of **BHC** and In^{3+}. Job plot and ESI-MS analyses drove us to propose the plausible binding mode of **BHC**-In^{3+} in Scheme 2.

With the result of fluorescence titration, detection limit using 3σ/slope was analyzed to be 0.89 μM ($R^2 = 0.9996$) (Fig. 5) [36]. Significantly, the detection limit is the lowest value among those previously known for fluorescent turn-on In^{3+} chemosensors, to date. (Table S1). Also, the association constant (K) based on Benesi-Hildebrand equation was turned out to be 4.3×10^3 M^{-1} (Fig. S5) [37].

For the practical application, the selectivity of compound **BHC** for In^{3+} was tested in the existence of other cations (Fig. S6). Hg^{2+} and Cu^{2+} inhibited the fluorescence of sensor **BHC**, and Fe^{3+} and Fe^{2+} displayed about half reduction of the fluorescence. Nevertheless, group 13 metals, Al^{3+} and Ga^{3+}, didn't show any fluorescence interferences.

Moreover, sensor **BHC** was applied to test strips. As shown in Fig. 6a, the obvious fluorescent emission appeared above 20 μM of In^{3+}. On the contrary, the same concentration of other cations did not show fluorescence emission (Fig. 6b). Therefore, it demonstrated that sensor **BHC** could be also used for detecting In^{3+} in the test strip.

To comprehend the detection mechanism of **BHC** towards In^{3+}, theoretical calculations were achieved. Based on the 1 to 1 binding stoichiometry between **BHC** and In^{3+}, energy-optimized structures and molecular orbital contributions of **BHC** and **BHC**-In^{3+} complex were calculated. As shown in Fig. 7a, sensor **BHC** displayed a bent form with the dihedral angle 33.384° for 1 N, 2 N, 3C, and 4O. Upon chelating to In^{3+}, its structure was flattened to 0.125° (Fig. 7b).

Based on these structures, molecular orbitals and transition energies were obtained by using TD-DFT calculation with the singlet excited states of **BHC** and **BHC**-In^{3+}. Thirty singlet states having non-zero oscillator strength were considered as allowed-transition. For **BHC**, the main absorption band was originated from the HOMO → LUMO transition (382.26 nm, Fig. S7), indicating ICT (intramolecular charge transfer)

transition from the naphthol group to the thiocyanate. In case of **BHC**-In^{3+}, the main absorption band was originated from the HOMO-1 → LUMO+1 and HOMO → LUMO+1 transitions (414.62 nm, Fig. S8). The electrons of both HOMO and HOMO-1 were mainly localized in the dibenzene ring, whereas those of LUMO+1 were localized in the naphthol moiety (Fig. S9). Their transitions indicated ICT and LMCT (ligand-to-metal charge-transfer). The decrease of the energy gap between HOMO and LUMO corresponded to red shift of the experimental UV-vis spectra.

From these results, the sensing mechanism of **BHC** towards In^{3+} maybe due to chelation-enhanced fluorescence (CHEF) effect. As In^{3+} bound to **BHC**, the rotation of imine (-C=N) was inhibited [38]. Therefore, the rigid structure and inhibited non-radiative transition could induce fluorescence enhancement.

Conclusion

In conclusion, we synthesized a fluorescence chemosensor **BHC** for detecting In^{3+} by a fluorescence turn-on method. It can obviously discriminate In^{3+} from the same group metals, Al^{3+} and Ga^{3+}, with no interferences. The detection limit for In^{3+} was 0.89 μM, which is the lowest among those previously known for fluorescent turn-on In^{3+} chemosensors, to date. Sensor **BHC** was also successfully applied to test strips. Moreover, fluorescence turn-on mechanism was proposed as chelation-enhanced fluorescence (CHEF) effect using DFT/TD-DFT calculation.

Acknowledgements The National Research Foundation of Korea (NRF) (NRF-2018R1A2B6001686) is thankfully acknowledged.

References

1. Asami T, Yoshino A, Kubota M, Gotoh S (1990) Background level of indium and gallium in soil with special reference to the pollution of the soils from zinc and lead smelters. J Plant Nutr Soil Sci 153: 257–259
2. Kho YM, Shin EJ (2017) Spiropyran-isoquinoline dyad as a dual chemosensor for Co(II) and In(III) detection. Molecules 22
3. Chen HW (2006) Gallium, indium, and arsenic pollution of groundwater from a semiconductor manufacturing area of Taiwan. Bull Environ Contam Toxicol 77:289–296
4. Han DY, Kim JM, Kim J, Jung HS, Lee YH, Zhang JF, Kim JS (2010) ESIPT-based anthraquinonylcalix[4]crown chemosensor for In^{3+}. Tetrahedron Lett 51:1947–1951
5. Wu Y-C, Li H-J, Yang H-Z (2010) A sensitive and highly selective fluorescent sensor for In^{3+}. Org Biomol Chem 8:3394–3397
6. Kim SK, Kim HS, Kim JH, Lee SH, Lee SW, Ko J, Bartsch RA, Kim JS (2005) indium(III)-induced fluorescent excimer formation and extinction in calix[4]arene-fluoroionophores. Inorg Chem 44: 7866–7875
7. Kim H, Kim KB, Song EJ, Hwang IH, Noh JY, Kim PG, Jeong KD, Kim C (2013) Turn-on selective fluorescent probe for trivalent cations. Inorg Chem Commun 36:72–76
8. Acar O, Türker AR, Kılıç Z (1998) Determination of bismuth, indium and lead in geological samples by electrothermal AAS. Fresenius J Anal Chem 360:645–649
9. Gęca I, Korolczuk M (2017) Sensitive anodic stripping Voltammetric determination of indium(III) traces following double deposition and stripping steps. J Electrochem Soc 164:H183–H187
10. Adya VC, Kumar M, Sengupta A, Natarajan V (2015) Inductively coupled plasma atomic emission spectrometric determination of indium (In) and gallium (Ga) in thorium matrix after chemical separation using Cyanex 923 extractant. At Spectrosc 36:261–265
11. Tehrani MH, Companys E, Dago A, Puy J, Galceran J (2018) Free indium concentration determined with AGNES. Sci Total Environ 612:269–275
12. Lee JJ, Park GJ, Kim YS, Lee SY, Lee JH, Noh I, Kim C (2015) A water-soluble carboxylic-functionalized chemosensor for detecting Al^{3+} in aqueous media and living cells: experimental and theoretical studies. Biosens Bioelectron 69:226–229
13. He G, Meng Q, Zhao X, He C, Zhou P, Duan C (2016) A new copper(II) selective fluorescence probe based on naphthalimide: synthesis, mechanism and application in living cells. Inorg Chem Commun 65:28–31
14. Park GJ, Lee JJ, You GR, Nguyen L, Noh I, Kim C (2016) A dual chemosensor for Zn^{2+} and Co^{2+} in aqueous media and living cells: experimental and theoretical studies. Sensors Actuators B Chem 223:509–519
15. Wu D, Sedgwick AC, Gunnlaugsson T, Akkaya EU, Yoon J, James TD (2017) Fluorescent chemosensors: the past, present and future. Chem Soc Rev 46:7105–7123
16. Ghosh P, Banerjee P (2017) Small molecular probe as selective tritopic sensor of Al^{3+}, F^- and TNP: fabrication of portable prototype for onsite detection of explosive TNP. Anal Chim Acta 965: 111–122
17. Huang L, Zhang J, Yu X, Ma Y, Huang T, Shen X, Qiu H, He X, Yin S (2015) A Cu^{2+}-selective fluorescent chemosensor based on BODIPY with two pyridine ligands and logic gate. Spectrochim Acta A 145:25–32
18. Lim C, An M, Seo H, Huh JH, Pandith A, Helal A, Kim HS (2017) Fluorescent probe for sequential recognition of Ga^{3+} and pyrophosphate anions. Sensors Actuators B Chem 241:789–799
19. Kim DH, Im YS, Kim H, Kim C (2014) Solvent-dependent selective fluorescence sensing of Al^{3+} and Zn^{2+} using a single Schiff base. Inorg Chem Commun 45:15–19
20. Maity D, Govindaraju T (2011) Naphthaldehyde-urea/Thiourea conjugates as turn-on fluorescent probes for Al^{3+} based on restricted C=N isomerization. Eur J Inorg Chem 2011:5479–5485
21. Goswami S, Manna A, Paul S, Maity AK, Saha P, Quah CK, Fun H-K (2014) FRET based 'red-switch' for Al^{3+} over ESIPT based 'green-switch' for Zn^{2+} : dual channel detection with live-cell imaging on a dyad platform. RSC Adv 4:34572–34576
22. Jang HJ, Kang JH, Yun D, Kim C (2018) A multifunctional selective "turn-on" fluorescent chemosensor for detection of group IIIA ions Al^{3+}, Ga^{3+} and In^{3+}. Photochem Photobiol Sci 17:1247–1255. https://doi.org/10.1039/C8PP00171E
23. Hu J-H, Li J-B, Sun Y, Pei P-X, Qi J (2017) A turn-on fluorescent chemosensor based on acylhydrazone for sensing of Mg^{2+} with a low detection limit. RSC Adv 7:29697–29701
24. Magde D, Wong R, Seybold PG (2002) Fluorescence quantum yields and their relation to lifetimes of rhodamine 6G and fluorescein in nine solvents: improved absolute standards for quantum yields. Photochem Photobiol 75:327–334
25. Long L, Huang M, Wang N, Wu Y, Wang K, Gong A, Zhang Z, Sessler JL (2018) A mitochondria-specific fluorescent probe for

visualizing endogenous hydrogen cyanide fluctuations in neurons. J Am Chem Soc 140:1870–1875

26. Frisch MJ, Trucks GW, Schlegel HB, Scuseria GE, Robb MA, Cheeseman JR, Scalmani G, Barone V, Mennucci B, Petersson GA, Nakatsuji H, Caricato M, Li X, Hratchian HP, Izmaylov AF, Bloino J, Zheng G, Sonnenberg JL, Hada M, Ehara M, Toyota K, Fukuda R, Hasegawa J, Ishida M, Nakajima T, Honda Y, Kitao O, Nakai H, Vreven T, Montgomery JA Jr, Peralta JE, Ogliaro F, Bearpark M, Heyd JJ, Brothers E, Kudin KN, Staroverov VN, Kobayashi R, Normand J, Raghavachari K, Rendell A, Burant JC, Iyengar SS, Tomasi J, Cossi M, Rega N, Millam JM, Klene M, Knox JE, Cross JB, Bakken V, Adamo C, Jaramillo J, Gomperts R, Stratmann RE, Yazyev O, Austin AJ, Cammi R, Pomelli C, Ochterski JW, Martin RL, Morokuma K, Zakrzewski VG, Voth GA, Salvador P, Dannenberg JJ, Dapprich S, Daniels AD, Farkas Ö, Foresman JB, Ortiz JV, Cioslowski J, Fox DJ (2009) Gaussian 09. Gaussian, Inc., Wallingford CT
27. Becke AD (1993) Density-functional thermochemistry. III. The role of exact exchange. J Chem Phys 98:5648–5652
28. Lee C, Yang W, Parr RG (1988) Development of the Colle-Salvetti correlation-energy formula into a functional of the electron density. Phys Rev B 37:785–789
29. Hariharan PC, Pople JA (1973) The influence of polarization functions on molecular orbital hydrogenation energies. Theor Chim Acta 28:213–222
30. Francl MM, Pietro WJ, Hehre WJ, Binkley JS, Gordon MS, DeFrees DJ, Pople JA (1982) Self-consistent molecular orbital methods. XXIII. A polarization-type basis set for second-row elements. J Chem Phys 77:3654–3665
31. Hay PJ, Wadt WR (1985) Ab initio effective core potentials for molecular calculations. Potentials for the transition metal atoms Sc to Hg. J Chem Phys 82:270–283
32. Wadt WR, Hay PJ (1985) Ab initio effective core potentials for molecular calculations. Potentials for main group elements Na to Bi. J Chem Phys 82:284–298
33. Lee SY, Bok KH, Kim C (2017) A fluorescence "turn-on" chemosensor for Hg^{2+} and ag^{+} based on NBD (7-nitrobenzo-2-oxa-1,3-diazolyl). RSC Adv 7:290–299
34. Vincenzo B, Cossi M (1998) Quantum calculation of molecular energies and energy gradients in solution by a conductor solvent model. J Phys Chem 102:1995–2001
35. Maurizio C, Vincenzo B (2001) Time-dependent density functional theory for molecules in liquid solutions. J Chem Phys 115:4708–4717
36. McNaught AD, Wilkinson A (1997) Limit of detection in analysis. IUPAC Compendium of Chemical Terminololy, 2nd edn. (the "Gold Book") Blackwell Scientific Publications, Oxford
37. Benesi HA, Hildebrand JH (1949) A spectrophotometric investigation of the interaction of iodine with aromatic hydrocarbons. J Am Chem Soc 71:2703–2707
38. Goswami S, Aich K, Das S, Das Mukhopadhyay C, Sarkar D, Mondal TK (2015) A new visible-light-excitable ICT-CHEF-mediated fluorescence 'turn-on' probe for the selective detection of Cd^{2+} in a mixed aqueous system with live-cell imaging. Dalton Trans 44:5763–5770